

Electrochemical Properties and Crystal Structure of Li⁺ / H⁺ Cation-exchanged LiNiO₂

Takahiro Toma^{1,2}, Ryo Maezono^{2,6}, and Kenta Hongo³⁻⁶

¹ Battery Research Laboratories Sumitomo Metal Mining Co., Ltd., Isoura-cho 17-3, Niihama, Ehime 792-0002, Japan

² School of Information Science, JAIST, Asahidai 1-1, Nomi, Ishikawa 923-1292, Japan

³ Research Center for Advanced Computing Infrastructure, JAIST, Asahidai 1-1, Nomi, Ishikawa 923-1292, Japan

⁴ PRESTO, Japan Science and Technology Agency, 4-1-8 Honcho, Kawaguchi-shi, Saitama 322-0012, Japan

⁵ Center for Materials Research by Information Integration, Research and Services Division of Materials Data and Integrated System,

National Institute for Materials Science, 1-2-1 Sengen, Tsukuba, Ibaraki 305-0047, Japan and

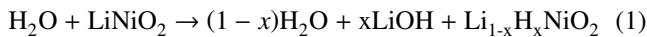
⁶ Computational Engineering Applications Unit, RIKEN, 2-1 Hirosawa, Wako, Saitama 351-0198, Japan

(Dated: January 1, 2020)

LiNiO₂ has high energy density but easily reacts with moisture in the atmosphere and deteriorates. We performed qualitative and quantitative evaluations of the degraded phase of LiNiO₂ and the influence of the structural change on the electrochemical properties of the phase. Li_{1-x}H_xNiO₂ phase with cation exchange between Li⁺ and H⁺ was confirmed by thermogravimetric analysis and Karl Fischer titration measurement. As the H concentration in LiNiO₂ increased, the rate capability deteriorated, especially in the low-temperature range and under low state of charge. Experimental and density functional theory (DFT) calculation results suggested that this outcome was due to increased activation energy of Li⁺ diffusion owing to cation exchange. Rietveld analysis of X-ray diffraction and DFT calculation confirmed that the *c* lattice parameter and Li-O layer reduced because of the Li⁺/H⁺ cation exchange. These results indicate that LiNiO₂ modified in the atmosphere has a narrowed Li-O layer, which is the Li diffusion path, and the rate characteristics are degraded.

I. INTRODUCTION

Increasing environmental awareness has raised the demand for vehicles with low CO₂ emissions. In recent years, global environmental concerns have accelerated the development and spread of hybrid electric vehicles (HEVs), plug-in hybrid electric vehicles, pure electric vehicles, and fuel-cell-based electric vehicles equipped with lithium-ion batteries (LIBs). LIBs installed in electric vehicles are required to have high energy density, rate capability, safety, and lifetime.¹ Ni-rich cathode active materials such as LiNiO₂²⁻⁵ and LiNi_xCo_yAl_zO₂⁶⁻¹¹ are used in automotive lithium ion secondary battery applications owing to their high energy density. However, Ni-rich cathode active materials have the problem that they easily react with moisture in the atmosphere, causing structural change of the material and generation of residual Li impurities such as LiOH, Li₂CO₃, and LiHCO₃. As a result, the Li⁺ insertion and desorption reactions with the active material are inhibited, and the electrochemical characteristics are deteriorated.¹¹⁻¹⁵ Regarding the structural change caused by the reaction between LiNiO₂ and H₂O, a structure in which Li and H are cation-exchanged as shown in eq (1) has been proposed.^{4,14} However, a result that confirms the existence of Li_{1-x}H_xNiO₂ experimentally has not been obtained.



One of the reasons why it is difficult to identify substances experimentally is the extremely low content of the target. Usually, X-ray powder diffraction is effective in identifying the generated heterogeneous phase, but if the amount of phase is very small, such as a phase that has been altered by exposure to the atmosphere, it may be impossible to evaluate it directly because it is below the detection limit of the measuring device.

Herein, we performed experimental and computational approaches, to find out the qualitative and quantitative identification of the structural phase of Li_{1-x}H_xNiO₂ and the investigation of its influence on the electrochemical properties. The qualitative and quantitative identifications of structural change phases were attempted by combining thermogravimetric analysis and Karl Fischer titration measurements. Although it may not be possible to clearly deduce the structural change phase itself in experiments, its influence on the electrochemical properties and lattice parameter can be clearly observed even with a small amount. Therefore, we simulated the crystal structure and electrochemical properties of Li_{1-x}H_xNiO₂ which was estimated structural change phase, using first-principles calculations and confirmed the agreement between the experimental and simulation results. This study is a new initiative that shows the effects of atmospheric exposure of cathode active materials on the crystal structure and electrochemical properties accurately and quantitatively, and proposes factor to be considered especially for Ni-rich cathode active materials.

II. EXPERIMENTAL METHODS

A. Substitution of Li⁺/H⁺ in LiNiO₂

LiNiO₂ samples were obtained by solid phase synthesis of Ni(OH)₂ and LiOH. Ni(OH)₂ precursors were synthesized by co-precipitation.¹⁶ A 2.0 M aqueous solution of NiSO₄ was pumped into a continuously stirred tank reactor in nitrogen atmosphere. The pH of the solution inside the reactor was controlled at approximately 11 by adding NaOH solution. NH₄OH solution, which acts as a chelating agent to

control the Ni ion neutralization reaction time, was separately pumped into the reactor. The $\text{Ni}(\text{OH})_2$ powder sample was washed, filtered, and dried in an oven at 120 °C for several hours. The prepared precursors were thoroughly mixed with LiOH powder at the ratio of $\text{Li}/\text{Ni} = 1.01$. The mixture was synthesized for 12 h at 710 °C in O_2 flow. The synthesized LiNiO_2 was placed in a chamber (LHL-113, ESPEC) maintained at 30 °C and 60% relative humidity under air circulation for 0, 9, 25, and 49 h. The four prepared LiNiO_2 samples are denoted as LNO_0 h, LNO_9 h, LNO_25 h, and LNO_49 h depending upon the exposure time.

LiNiO_2 contains LiOH and Li_2CO_3 produced by exposure to the atmosphere; therefore, the effects of the structural change phase and the residual Li compounds cannot be distinguished. In order to isolate the influence of the structural change phase, we attempted to remove the residual Li compound by washing the active material. The solvent used for removing the residual Li compound should be selected by considering its reactivity with LiNiO_2 . For example, excessive extraction of Li (eq. (1)) from the bulk can occur by using water as the solvent. Excessive delithiation causes significant degradation of the electrochemical properties,^{4,17} making it difficult to evaluate the effects of atmospheric exposure properly. Therefore, we used ethanol, which has poor reactivity with Li, as the washing solvent. To obtain LiNiO_2 without residual Li compound, 10 g LiNiO_2 powder was added to 200 mL of distilled ethanol under constant stirring with a magnetic stirrer for 5 min.

B. Material characterization

The surface morphologies of the samples were observed by field emission scanning electron microscopy (FE-SEM, JSM-7001, JEOL). The phase transformation of the surface layer was observed by spherical-aberration-corrected scanning transmission electron microscopy (CS-STEM, JEM-ARM200F, JEOL). The samples were sliced to a thickness of 100 nm or less using a focused ion beam (FIB, NIB-5000, Hitachi), and the samples were observed under the acceleration voltage of 200 kV. The crystalline phases of the prepared samples were identified using X-ray powder diffractometer (XRD, X'Pert Pro MPD, PANalytical) with $\text{Cu-K}\alpha$ radiation. The XRD data pattern was recorded at the scan rate of 5° min^{-1} in the 2θ range of 15° to 100° . Rietan-FP software¹⁸ was used for Rietveld analysis. The thermal behavior of the LiNiO_2 samples were investigated by thermogravimetric analysis (TGA) (DSCX3100SA, NETSZCH). Karl Fischer (KF) titration (CA-200, MITSUBISHI CHEMICAL ANALYTICAL) was used to evaluate to H_2O concentration.

C. Electrochemical techniques

Electrochemical measurements were carried out with a laminated-type full cell and CR2032 coin-type symmetric cell with positive electrodes facing each other. These cells were

used for rate capability test and electrochemical impedance spectroscopy (EIS) measurement, respectively. Each LiNiO_2 sample was mixed with a conducting agent (carbon black) and polyvinylidene fluoride (PVDF) at 85:10:5 weight ratio in N-methyl-2-pyrrolidone (NMP) to prepared a slurry. Then, each slurry was applied to an aluminum current collector and dried in a vacuum oven for 8 h at 120 °C. The dried coating foil was then compressed to a layer of 20 μm thickness using a roll press. Cu foil coated with graphite was used as the negative electrode in the laminate type cell. The electrolyte was 1.0 M LiPF_6 in ethylene carbonate (EC) - dimethyl carbonate (DMC) solution (3:7 by volume). For the rate capability test of the laminate-type cells, discharge rates at different current densities varying from 0.1 to 10C were applied using constant current (CC) with fixed charge rate of 0.1C and constant current - constant voltage (CC-CV) within the voltage range from 2.5 to 4.2 V at 25 °C. EIS measurements of the symmetric cells were carried out by applying an AC - amplitude of 10 mV at 100 kHz to 1 mHz frequency between -20 °C and 45 °C. The resulting Nyquist plots were analyzed using ZView software (Scribner Associates, Inc.).

D. Computational Methodology

All first-principles calculations using DFT were performed with the Vienna Ab initio Simulation Package (VASP)^{19,20} with projector augmented wave (PAW) potentials. A plane-wave basis set cutoff energy of 650 eV and a Monkhorst-Pack $3 \times 3 \times 1$ k-points mesh was used for all calculations. The calculation was performed using a supercell constructed from the primitive cell by tripling the system along the directions of the a and b axes. Energy optimizations were based on the tetrahedron method with Blöchl corrections for Brillouin-zone integrations; their convergence criteria for the self-consistent field (SCF) and maximum force were set to 0.1 meV/atom and 1.0 meV/Å, respectively. We adopted the optB86b-vdW functional²¹⁻²³ as the exchange-correlation (XC) functional because it is known to accurately reproduce experimental results such as voltage and volume in the Li detachment state. Considering the Coulomb interaction of the Ni $3d$ orbit, a correction of $U = 6.7\text{eV}$ was added to Ni $3d$.²⁴ In this study, the structural configuration was drawn using VESTA software.²⁵ In the structure relaxation calculation of the Li desorption structure, all symmetry structures that are Li defect sites were calculated, and the lowest energy configuration was defined as the Li desorption structure. The climbing image nudged elastic band (CI-NEB) method was used to determine the Li-ion diffusion barriers and paths.^{26,27} The initial and final configurations were determined by separately optimizing the structure with a vacancy at each of the two adjacent sites. A group of images generated by linear interpolation between the two endpoint configurations was optimized to converge to points on the minimum energy path. The five intermediate images between the two endpoints were generated by linear interpolation between the two endpoint configurations. The convergence criterion used in the CI-NEB calculations was that the forces acting on each atom was lesser than 0.02 meV/Å.

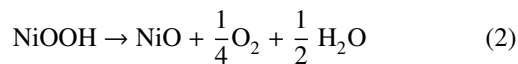
III. RESULTS AND DISCUSSION

A. Characterization

SEM and STEM observations were performed to evaluate the changes in the primary and secondary particles and surface structure changes before and after exposure to the atmosphere and washing. Each sample was confirmed to be free of primary and secondary particle size changes, particle collapse, and deformation (Figure 1(a)-(j)). On the other hand, the particle surface changed smoothly as the exposure time to the atmosphere increased, suggesting structural changes due to exposure. In the HAADF-STEM images of the particle surface (Figure 1(k)-(l)), layered stripes representing the $R\bar{3}m$ structure of LiNiO_2 were observed both inside and on the surface of pristine (k) and LNO_0 h(l). The results also confirmed that the washing process in this study removed the residual Li compound without changing the structure of the active material. In contrast, the LNO_9 h(m), LNO_25 h(n), and LNO_49 h(o) samples had altered layers with thickness of approximately 1 nm on the outermost surface. This alteration phase on the outermost surface was suggested to be NiO with $Fm\bar{3}m$ structure caused by the change in the arrangement of Ni atoms.²⁸⁻³² Because the NiO thickness was almost constant regardless of the samples exposed to the atmosphere, the influence of NiO is considered not to appear as a difference between the samples in the results of the electrochemical evaluation described later.

TGA analysis was performed to identify the structural change phases owing to phenomena such as thermal decomposition and oxidation. Figure 2 shows the TGA results of LiNiO_2 after atmospheric exposure.

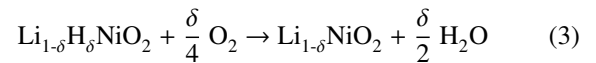
Weight loss from approximately 100-120 °C indicates water adsorption-desorption reactions. In the higher temperature region, large weight loss peaks were observed at 200–220 °C and 300–320 °C. These weight change peaks have been reported to be due to H_2O and O_2 elimination from NiOOH , as shown in eq. (2).^{33,34} $\text{Ni}(\text{OH})_2$ and NiOOH may also be generated by the mixing of Li^+/H^+ . However, the $\text{Ni}(\text{OH})_2$ decomposition temperature is approximately 300°C, and the existence of one weight loss peak has been reported.^{35,36} Therefore, the phase generated by atmospheric exposure is considered to be NiOOH .



Because LiNO_0h had little weight reduction reaction in the temperature ranges of 200–220 °C and 300–320 °C, the amount of NiOOH in the active material is considered to be small. On the other hand, in LNO_9h and LNO_49h, two peak changes at 200 °C or higher increased with increasing exposure time. From these results, it was suggested that the cation exchange of Li^+/H^+ proceeded at atmospheric exposure, and the production of NiOOH increased.

TGA can estimate the relationship between temperature and weight change reaction, but it is difficult to identify and quantitatively analyze the reacted substance. Therefore, quantitative analysis of the amount of NiOOH , that is, the amount

of H^+ exchange, was attempted by quantifying the amount of H_2O produced by the reaction in eq.(2). In order to separate the amount of H_2O derived from the adsorbed water and the amount of H_2O derived from the decomposition reaction of NiOOH , KF titration analysis was performed under two conditions of 120 °C and 300 °C. Titration at 120 °C detects the adsorbed water, and that at 300 °C detects the total amount of H_2O generated by decomposition of adsorbed water and NiOOH . Therefore, the amount of H_2O derived from the decomposition of NiOOH can be determined by taking the difference between the titration results of 300 °C (KF 300°C) and 120 °C (KF 120°C). Figure 3 shows the results of KF titration. The value of $\text{KF}300^\circ\text{C}-\text{KF}120^\circ\text{C}$ increased in proportion to the square root of the exposure time, that is, the amount of NiOOH produced increased with the exposure time. We assumed that the H desorption reaction was due to heating during KF titration, as expressed in eq.(3). In this case, the amount of H contained in LiNiO_2 can be calculated as shown in eq.(4) by using the amount of H_2O derived from NiOOH , $\alpha_{\text{H}_2\text{O}}$ ($\Delta \text{KF } 300^\circ\text{C} - \text{KF } 120^\circ\text{C}$). The H concentrations of LNO_0 h, LNO_9 h, LNO_25 h, and LNO_49 h were determined to be 0.08, 0.28, 0.40, and 0.51 at%, respectively.



$$\frac{\delta}{2} = \frac{\alpha_{\text{H}_2\text{O}} \cdot M_{\text{LiNiO}_2}}{M_{\text{H}_2\text{O}}} \quad (4)$$

XRD evaluation was performed to investigate the crystal structure change due to cation exchange of Li^+/H^+ . Figure 4(a),(b) shows the XRD profile of each sample. From the results of Fig. 4(a), it was confirmed that no significant heterogeneous formation was observed in any sample, and LiNiO_2 was the main phase. The (003) diffraction peak near 18.8°, i.e., the 3a site (Li site) in the $R\bar{3}m$ structure, showed a shift of the diffraction angle toward the higher angle side with increasing atmospheric exposure time (Figure 4(b)). In order to verify whether this peak shift was caused by Li^+/H^+ cation exchange, the XRD peak of $\text{Li}_{1-x}\text{H}_x\text{NiO}_2$ was simulated using first principles calculations. Figure 4(c), (d) shows the XRD profiles calculated for the crystal structure of LiNiO_2 obtained by structural relaxation calculation with Li replaced by 0 at%, 3.7 at%, and 100 at% of H. Similar to the experimental results, the relationship between the H content and the shift of the (003) peak position was also confirmed by calculation. From these results, it was found that the (003) peak position shifts to the higher angle side due to the exchange of Li^+/H^+ , i.e., the *c*-axis lattice constant shrinks. In addition, the lattice constants obtained by Rietveld analysis and first-principles calculation are summarized in Table I.

B. Electrochemical properties

Rate capability test results measured at different current densities (0.1–10C) are shown in Figure 5. At low discharge rate (0.1–1C), all samples showed almost the same discharge

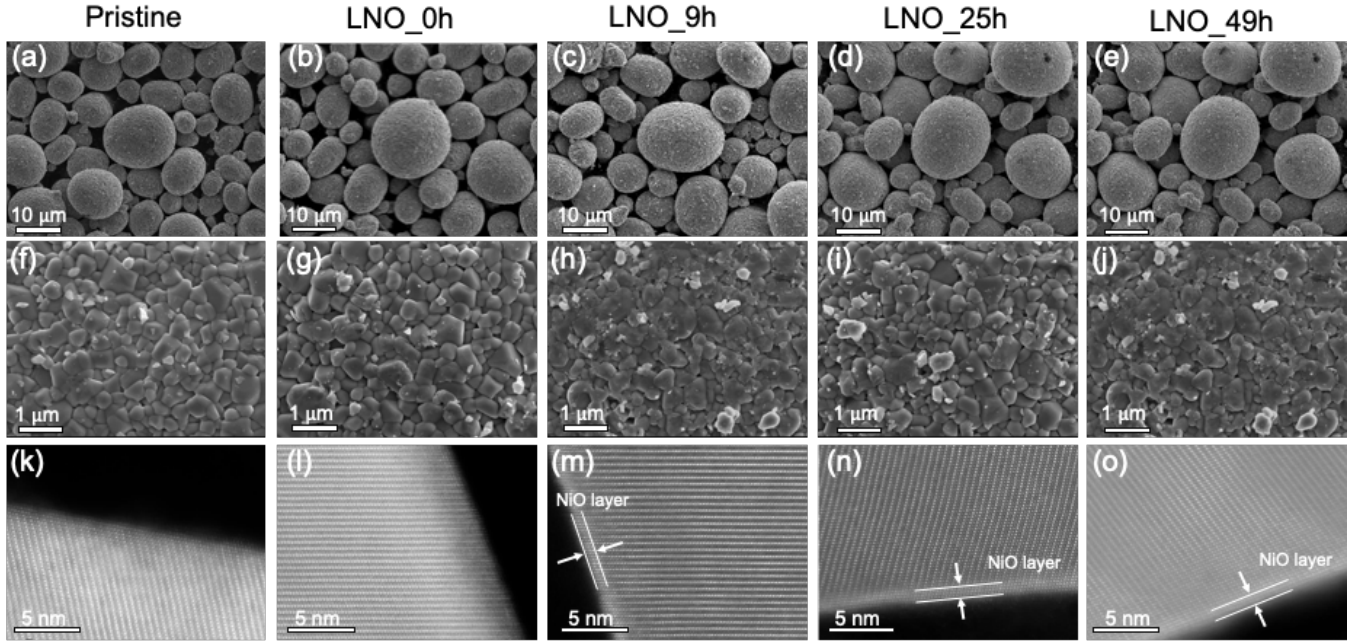


FIG. 1. Low-magnification surface SEM images (a)-(e) and high-magnification SEM images (f)-(j) of the samples. Cross-sectional HAADF-STEM images ((k)-(o)). (a),(f),(k) Pristine samples (no exposure to air, no washing); (b),(g),(l) LNO_0 h; (c),(h),(m) LNO_9 h; (d),(i),(n) LNO_25 h; and (e),(j),(o) LNO_49 h panels.

TABLE I. Lattice constant of Li^+/H^+ cation exchange structure obtained by Rietveld analysis and first-principles calculation

Samples	H (at%)	a (Å)	c (Å)
LNO_0h	0.08	2.8776	14.2057
LNO_9h	0.28	2.8766	14.2005
LNO_25h	0.40	2.8761	14.1988
LNO_49h	0.51	2.8755	14.1962
LiNiO_2 (calc)	0	2.8500	14.1966
$\text{Li}_{0.96}\text{H}_{0.04}\text{NiO}_2$ (calc)	3.70	2.8446	14.1052
HNiO_2 (calc)	100	2.7554	12.9179

capacity. On the other hand, at high discharge rate (3–10C), a significant decrease in the discharge capacity was confirmed in the LNO_25 h and LNO_49 h samples. This result implies that a material with a large amount of Li^+/H^+ is slow to exhibit the Li^+ transfer reaction at high discharge rate.

EIS measurements were carried out to investigate the electrochemical resistance. In this study, the positive electrode resistance was measured using a symmetric coin cell with the positive electrodes facing each other. The resistance components of the cathode and anode are intermixed in the impedance spectrum of a normal full cell, and distinguishing the resistance of the positive electrode alone is difficult. Furthermore, in order to evaluate the relationship between the amount of Li contained in LiNiO_2 and the resistance, measurements were performed under the conditions of $\text{Li}_{0.50}\text{NiO}_2$ and $\text{Li}_{0.75}\text{NiO}_2$. In addition, EIS measurements were performed under four conditions of 253, 273, 298, and 318 K to obtain the temperature dependence of Li^+ diffusion coefficient

and the activation energy of the diffusion. Figure 6 and Figure 7 show the Nyquist plots of $\text{Li}_{0.50}\text{NiO}_2$ and $\text{Li}_{0.75}\text{NiO}_2$, respectively. In $\text{Li}_{0.50}\text{NiO}_2$, the charge transfer resistance (R_{ct}) increased with increase in the amount of Li^+/H^+ cation exchange in the temperature range of 253–318 K. On the other hand, in $\text{Li}_{0.75}\text{NiO}_2$, R_{ct} markedly increased in the LNO_25 h and LNO_49 h samples in the low-temperature region of 253 K, but no significant difference in R_{ct} was observed in any sample in the region of 273–318 K. To summarize these results, the higher the Li concentration in LiNiO_2 or the lower the operating temperature, the greater the effect on Li insertion reaction due to Li^+/H^+ cation exchange. Some studies have shown that the increase in resistance in the low-temperature range is caused by a decrease in the diffusion rate of Li^{+37-39} and the relationship between the Li concentration in the bulk and the diffusion coefficient of Li^+ .^{40,41} Therefore, we believe that the $\text{Li}_{1-x}\text{H}_x\text{NiO}_2$ phase that underwent structural change due to atmospheric exposure affected the Li^+ diffusion.

The diffusion region of the EIS spectrum was analyzed to obtain the Li diffusion coefficient of each sample. The linear behavior in the low-frequency region of the EIS spectrum shows the Li^+ diffusion behavior, and the Li^+ diffusion coefficient D_{Li^+} is calculated using the expression eq.(5).^{39,42-45}

$$D_{\text{Li}^+} = \frac{R^2 T^2}{2A^2 n^4 F^4 C^2 \sigma^2}, \quad (5)$$

where R denotes the gas constant, T is the absolute temperature, A is the area of the cathode/electrolyte interface ($A = 1.33\text{cm}^2$), n is the charge number of the electroactive species ($n=1$), F is Faraday's constant, C is the concentration of

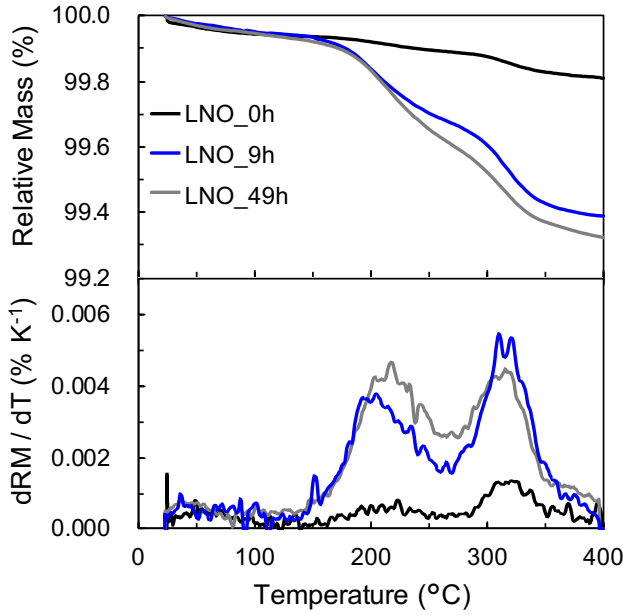


FIG. 2. Normalized thermogravimetric rate of change of LiNiO_2 exposed to air for 0 h, 9 h, and 49 h. The upper panel shows the results of heating from 25 °C to 400 °C in Ar atmosphere. The lower panel shows the result of differentiating the weight change rate with temperature ($d\text{RM}/dT$).

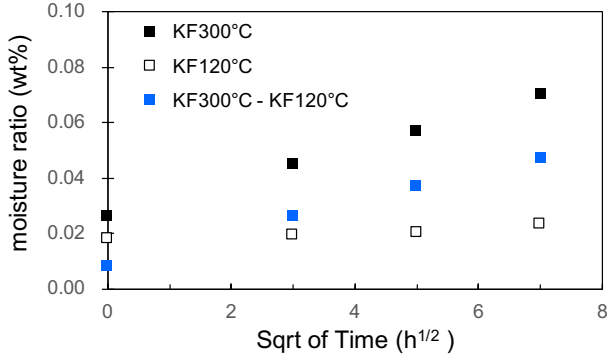


FIG. 3. Relationship between atmospheric exposure time and moisture content of LiNiO_2 . The black square and the white square are the titration results at 300 °C and 120 °C, respectively. The blue square shows the difference between the results at 300 °C and 120 °C.

lithium ion, and σ is the Warburg factor. The Warburg factor was obtained from the slope of the plots of Z' vs $\omega^{-1/2}$ (ω is the angular frequency) in the Warburg region.⁴³ D_{Li^+} obtained by the formula (5) is shown in Figure 8. D_{Li^+} increased with rising temperature, and the calculated value of D_{Li^+} was in good agreement with the previously reported LiNiO_2 measurement result.^{46,47}

Furthermore, we derived the activation energy of diffusion using the following Arrhenius equation.^{39,46,48,49}

$$D_{\text{Li}^+} = D_0 \exp\left(\frac{E_a}{RT}\right) \quad (6)$$

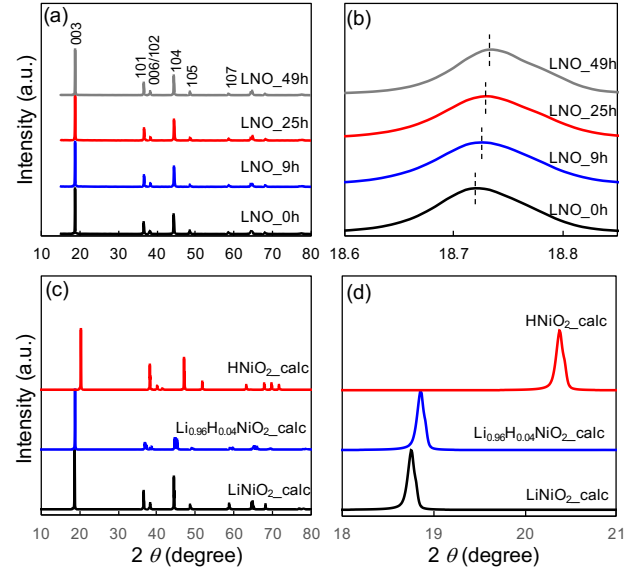


FIG. 4. Panel (a) shows the entire XRD profile of each sample, and panel (b) shows an enlarged view near the (003) diffraction angle. Panel (c) shows the result of simulating the XRD profile of LiNiO_2 with 0, 3.7, and 100 at% substitution of Li with H by DFT calculation, and panel (d) is an enlarged graph of (003) diffraction angle of profile (c).

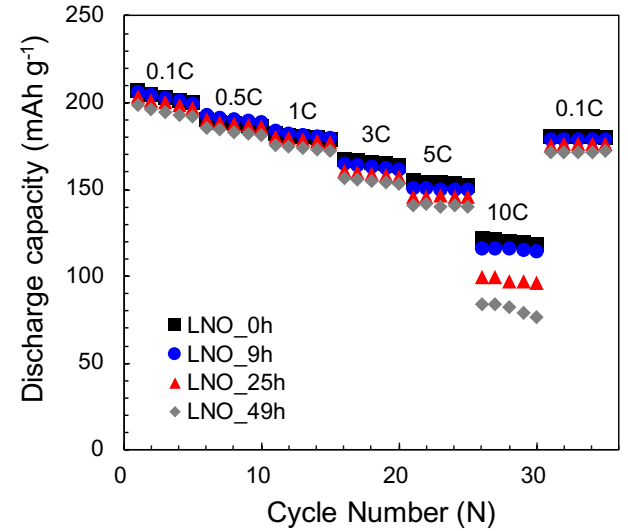


FIG. 5. Rate characteristics measured at different rates of 0.1–10C. The samples are denoted as black square (LNO.0 h), blue circle (LNO.9 h), red triangle (LNO.25 h), and gray rhombus (LNO.49 h).

The determined activation energy (E_a) is shown in Table II. Increase in E_a was confirmed by increasing Li concentration in LiNiO_2 and decreasing temperature, and this result corresponded to the EIS spectrum variation. Therefore, the influence of Li^+/H^+ cation exchange on the electrochemical properties (increased resistance and degradation of rate capability) is attributed to the increase in the activation energy of Li^+ dif-

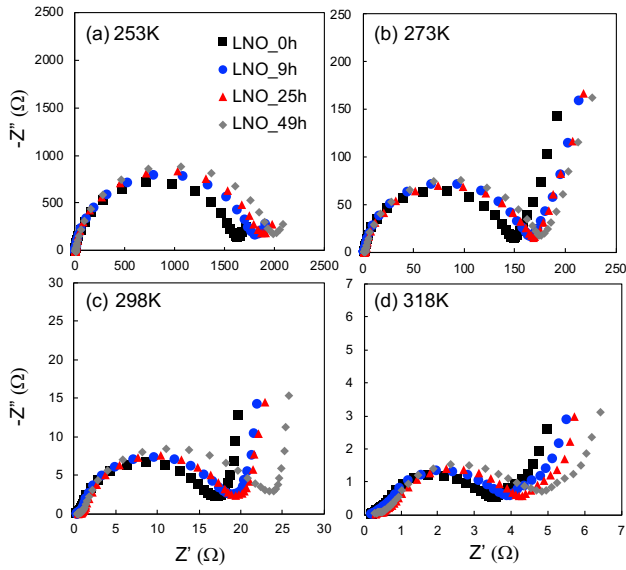


FIG. 6. EIS spectrum of $\text{Li}_{0.50}\text{NiO}_2$ at (a) 253 K, (b) 273 K, (c) 298 K, (d) 318 K

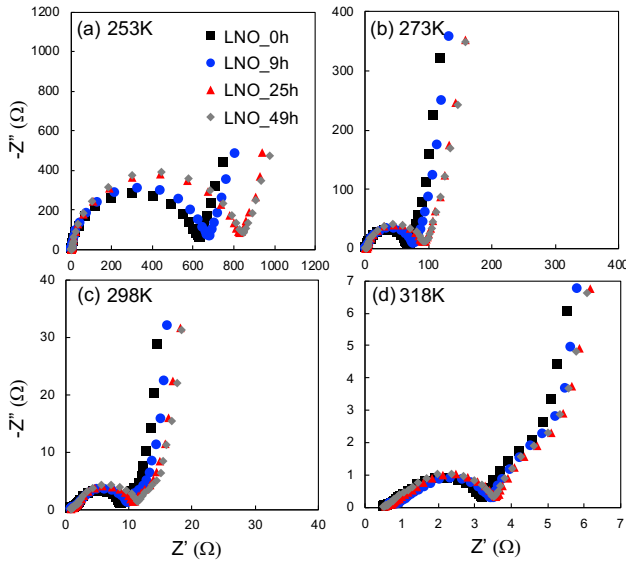


FIG. 7. EIS spectrum of $\text{Li}_{0.75}\text{NiO}_2$. Each panel shows the results of (a) 253 K, (b) 273 K, (c) 298 K, (d) 318 K

fusion.

To further verify whether the change in activation energy was due to the effect of Li^+/H^+ cation exchange, the barrier energy for Li^+ diffusion in $\text{Li}_{1-x}\text{H}_x\text{NiO}_2$ was calculated by the CI-NEB method. The calculation was performed using a structure in which one of the 27 Li atoms contained in the supercell was replaced with an H atom ($x = 0.037$). In addition, the barrier energies of $\text{Li}_{0.481}\text{H}_{0.037}\text{NiO}_2$ and $\text{Li}_{0.741}\text{H}_{0.037}\text{NiO}_2$, which are close to the amount of Li desorption in the experiment, were calculated. Figure 9(a)(b) shows the Li^+ diffusion paths of $\text{Li}_{0.481}\text{NiO}_2$ as an example of the calculated structure. The energy

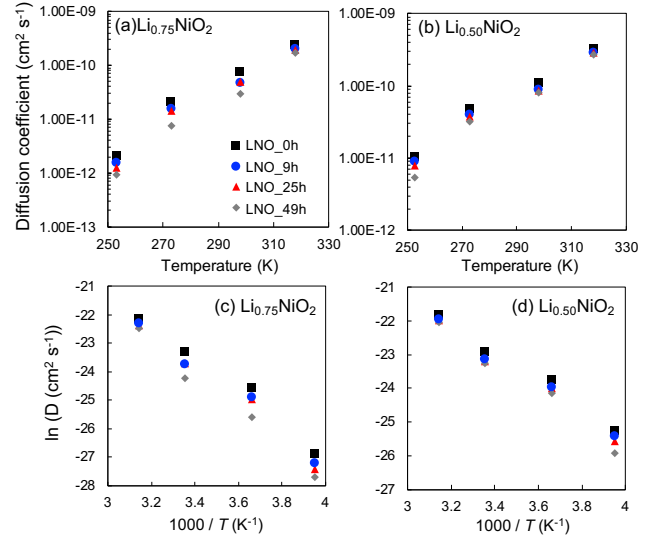


FIG. 8. Li^+ diffusion coefficient determined from EIS measurement. The temperature dependences of D_{Li^+} in $\text{Li}_{0.75}\text{NiO}_2$ and $\text{Li}_{0.50}\text{NiO}_2$ are shown in (a) and (b), respectively. Panels (c) and (d) show the Arrhenius plots of D_{Li^+} for $\text{Li}_{0.75}\text{NiO}_2$ and $\text{Li}_{0.50}\text{NiO}_2$, respectively.

TABLE II. Relationship between activation energy and exposure time (Li^+/H^+ exchange amount) in $\text{Li}_{1-x}\text{NiO}_2$ ($x = 0.25, 0.50$)

Sample	E_a (eV)			
	LNO_0h	LNO_9h	LNO_25h	LNO_49h
$\text{Li}_{0.75}\text{NiO}_2$	0.488	0.498	0.518	0.534
$\text{Li}_{0.50}\text{NiO}_2$	0.351	0.351	0.364	0.396

profiles of $\text{Li}_{0.741}\text{NiO}_2$, $\text{Li}_{0.741}\text{H}_{0.037}\text{NiO}_2$, $\text{Li}_{0.481}\text{NiO}_2$, and $\text{Li}_{0.481}\text{H}_{0.037}\text{NiO}_2$ are shown in Figure 9(c); the barrier energies were determined to be 0.567, 0.760, 0.193, and 0.286 eV, respectively. At the Li concentrations of $(1-x) = 0.48$ and 0.75, the barrier energy increased with increase in the H^+ concentration in LiNiO_2 , and the same tendency as observed in the experimental results was obtained. In literature⁵⁰, the barrier energy of $\text{Li}_{0.50}\text{NiO}_2$ is reported as approximately 0.20–0.30 eV, and the calculation result of $\text{Li}_{0.481}\text{NiO}_2$ shows a close value (0.193 eV).

After structural relaxation calculation, Figure 10 shows that O atoms are attracted to H atom in the Li-O layer of $\text{Li}_{0.963}\text{H}_{0.037}\text{NiO}_2$. In NiOOH , it has been reported^{51–54} that the NiO_2 and Ni(OH)_2 slabs are alternately stacked by bonding through hydrogen bonds. From the reported phenomenon, it is presumed that the H atoms in the Li-O layer cause an attractive action in the form of hydrogen bonds between the upper and lower NiO_2 slabs, resulting in the shrinkage of the Li-O layer thickness. In addition, the inverse relationship between the Li-O layer thickness and the activation energy is known,⁵⁰ which is presumed to be the cause of increase in the activation energy due to Li^+/H^+ cation exchange.

Furthermore, we investigated changes in the c lattice constant, Li-O layer thickness, and Ni-O layer thickness with respect to the amount of Li desorption in Li_xNiO_2 and

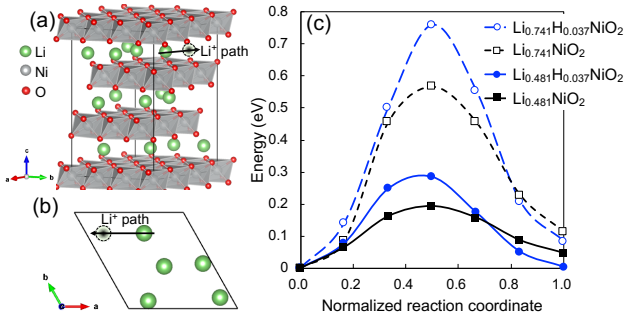


FIG. 9. (a): Li^+ diffusion path of $\text{Li}_{0.481}\text{NiO}_2$ by CI-NEB calculation, (b): (a) Top view of the Li layer, where the Li diffusion path exists in the c -axis direction (c) Energy profiles of Li diffusion path determined by CI-NEB.

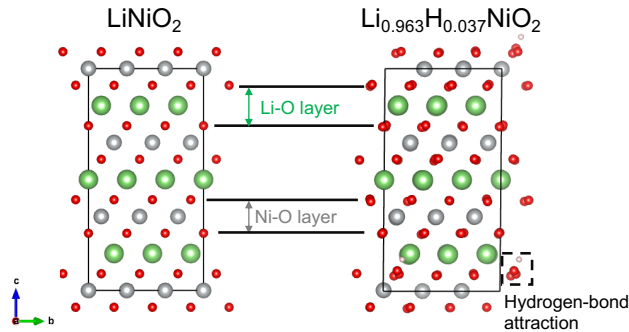


FIG. 10. Crystal structure of LiNiO_2 and $\text{Li}_{0.963}\text{H}_{0.037}\text{NiO}_2$ after structural relaxation.

$\text{Li}_x\text{H}_{0.037}\text{NiO}_2$. The structures in which Li was sequentially desorbed one after the other were determined by DFT calculation, and the parameters for each structure were obtained. Li_xNiO_2 has larger c lattice parameter than $\text{Li}_x\text{H}_{0.037}\text{NiO}_2$ in the region of $x = 0.4\text{--}1.0$ (Figure 11(a)). Based on the trend of the change in the layer thicknesses of the Li-O layer and Ni-O layer, it was confirmed that the change in the c -axis lattice constant due to Li^+/H^+ cation exchange was dominated by the change in thickness of the Li layer (Figure 11(b),(c)). This result agrees with the change in the activation energy determined by the experiment and CI-NEB method.

IV. SUMMARY

The structural changes and their effects on the electrochemical properties of LiNiO_2 exposed to the atmosphere were investigated. Thermal and chemical analyses revealed that LiNiO_2 exposed to the atmosphere assumes the structure of $\text{Li}_{1-x}\text{H}_x\text{NiO}_2$ with Li^+/H^+ cation exchange. We synthesized LiNiO_2 with different amounts of H^+ exchange, and investigated the influence of $\text{Li}_{1-x}\text{H}_x\text{NiO}_2$ on the electrochemical properties. As a result, it was found that the activation energy of Li^+ diffusion increased by the exchange of H^+ , resulting in higher resistance and lower rate capability. Our first principles

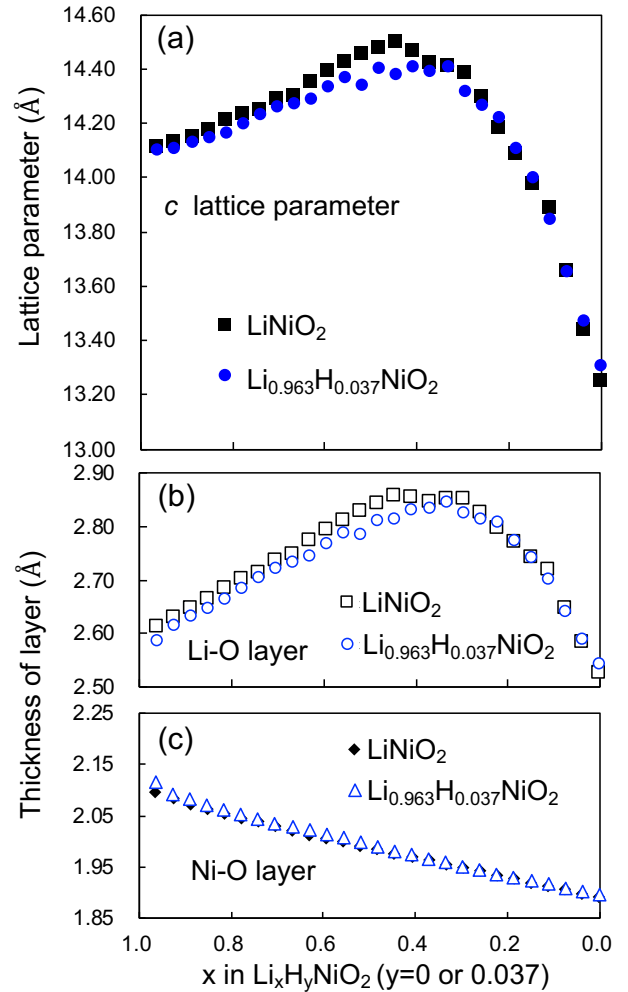


FIG. 11. (a): Relationship between Li concentration and c -axis lattice constant of $\text{Li}_x\text{H}_y\text{NiO}_2$. Panels (b) and (c) show the relationship between the amount of Li desorption and the change in thickness of the Li-O and Ni-O layers, respectively.

analysis calculation revealed that the increase in the activation energy was caused by decrease in the Li layer thickness, that is, constriction of the diffusion path of Li^+ .

V. ACKNOWLEDGMENTS

T. T. is deeply grateful to K. Ryoshi and T. Yoshida for their fruitful discussions and technical support. The computations in this work were performed using the facilities of Research Center for Advanced Computing Infrastructure at JAIST. K. H. is grateful for the financial support from KAKENHI (grant numbers 17K17762 and 19K05029), Grant-in-Aid for Scientific Research on Innovative Areas (16H06439 and 19H05169), the FLAG-SHIP2020 project (MEXT for computational resources, projects hp190169 and hp190167 using K-computer), PRESTO (JPMJPR16NA), and Materials research by Information Integration Initia-

tive (MI²I) project of the Support Program for Starting Up Innovation Hub from Japan Science and Technology Agency (JST). R. M. is grateful for financial support from MEXT-KAKENHI (projects JP19H04692 and JP16KK0097),

the FLAG-SHIP2020 project (MEXT for computational resources, projects hp190169 and hp190167 using K-computer), and the Air Force Office of Scientific Research (AFOSR-AOARD/FA2386-17-1-4049;FA2386-19-1-4015).

- ¹ J. Neubauer, A. Pesaran, C. Bac, R. Elder, and B. Cunningham, *J. Power Sources* **271**, 614 (2014).
- ² T. Ohzuku, A. Ueda, and M. Nagayama, *J. Electrochem. Soc.* **140**, 1862 (1993).
- ³ P. Kalyani and N. Kalaiselvi, *Sci. Technol. Adv. Mater.* **6**, 689 (2005).
- ⁴ R. Moshtev, P. Zlatilova, S. Vasilev, I. Bakalova, and A. Kozawa, *J. Power Sources* **81-82**, 434 (1999).
- ⁵ T. Ohzuku, A. Ueda, and M. Kouguchi, *J. Electrochem. Soc.* **142**, 4033 (1995).
- ⁶ S. P. Lin, K. Z. Fung, Y. M. Hon, and M. H. Hon, *J. Solid State Chem.* **167**, 97 (2002).
- ⁷ X. Zhu, H. Chen, H. Zhan, D. Yang, and Y. Zhou, *Mater. Chem. Phys.* **88**, 145 (2004).
- ⁸ S. H. Park, K. S. Park, Y. Sun Kook, K. S. Nahm, Y. S. Lee, and M. Yoshio, *Electrochim. Acta* **46**, 1215 (2001).
- ⁹ W. Li and J. C. Currie, *J. Electrochem. Soc.* **144**, 2773 (1997).
- ¹⁰ K. K. Lee, W. S. Yoon, K. B. Kim, K. Y. Lee, and S. T. Hong, *J. Power Sources* **97-98**, 308 (2001).
- ¹¹ H. Liu, Y. Yang, and J. Zhang, *J. Power Sources* **162**, 644 (2006).
- ¹² K. Matsumoto, R. Kuzuo, K. Takeya, and A. Yamanaka, *J. Power Sources* **81-82**, 558 (1999).
- ¹³ H. Liu, Y. Yang, and J. Zhang, *J. Power Sources* **173**, 556 (2007).
- ¹⁴ N. V. Faenza, L. Bruce, Z. W. Lebens-Higgins, I. Plitz, N. Pereira, L. F. Piper, and G. G. Amatucci, *J. Electrochem. Soc.* **164**, A3272 (2017).
- ¹⁵ X. Zhang, W. J. Jiang, X. P. Zhu, A. Mauger, Qilu, and C. M. Julien, *J. Power Sources* **196**, 5102 (2011).
- ¹⁶ S. Huang, H. Wu, P. Chen, Y. Guo, B. Nie, B. Chen, H. Liu, and Y. Zhang, *J. Mater. Chem. A* **3**, 3633 (2015).
- ¹⁷ S. Xu, C. Du, X. Xu, G. Han, P. Zuo, X. Cheng, Y. Ma, and G. Yin, *Electrochim. Acta* **248**, 534 (2017).
- ¹⁸ F. Izumi and K. Momma, *Solid State Phenom.* **130**, 15 (2007).
- ¹⁹ G. Kresse and J. Furthmüller, *Comput. Mater. Sci.* **6**, 15 (1996).
- ²⁰ G. Kresse and J. Furthmüller, *Phys. Rev. B* **54**, 11169 (1996).
- ²¹ J. Klime, D. R. Bowler, and A. Michaelides, *Phys. Rev. B* **83**, 1 (2011).
- ²² T. Yoshida, K. Hongo, and R. Maezono, *J. Phys. Chem. C* **123**, 14126 (2019).
- ²³ M. D. Radin and A. Van Der Ven, *Chem. Mater.* **28**, 7898 (2016).
- ²⁴ F. Zhou, M. Cococcioni, C. A. Marianetti, D. Morgan, and G. Ceder, *Phys. Rev. B* **70**, 1 (2004).
- ²⁵ K. Momma and F. Izumi, *J. Appl. Crystallogr.* **44**, 1272 (2011).
- ²⁶ G. Henkelman and H. Jónsson, *J. Chem. Phys.* **113**, 9978 (2000).
- ²⁷ G. Henkelman, B. P. Uberuaga, and H. Jónsson, *J. Chem. Phys.* **113**, 9901 (2000).
- ²⁸ W. Lee, S. Muhammad, T. Kim, H. Kim, E. Lee, M. Jeong, S. Son, J. H. Ryou, and W. S. Yoon, *Adv. Energy Mater.* **8**, 1 (2018).
- ²⁹ Y. Cho, P. Oh, and J. Cho, *Nano Lett.* **13**, 1145 (2013).
- ³⁰ T. Hayashi, J. Okada, E. Toda, R. Kuzuo, N. Oshimura, N. Kuwata, and J. Kawamura, *J. Electrochem. Soc.* **161**, 1007 (2014).
- ³¹ Y. Makimura, S. Zheng, Y. Ikuhara, and Y. Ukyo, *J. Electrochem. Soc.* **159**, 1070 (2012).
- ³² B. Huang, D. Liu, K. Qian, L. Zhang, K. Zhou, Y. Liu, F. Kang, and B. Li, *ACS Appl. Mater. Interfaces* **11**, 14076 (2019).
- ³³ H. M. Gu, W. Wang, and Y. C. Zhai, *Adv. Mater. Res.* **239-242**, 646 (2011).
- ³⁴ J. Pan, Y. Sun, P. Wan, Z. Wang, and X. Liu, *Electrochem. Commun.* **7**, 857 (2005).
- ³⁵ A. Tang, X. Li, Z. Zhou, O. Jing, and H. Yang, *J. Alloys Compd.* **600**, 204 (2014).
- ³⁶ Z. F. Zhu, N. Wei, H. Liu, Z. L. He, and D. Yang, *Adv. Powder Technol.* **42**, 436 (2011).
- ³⁷ S. Y. Tan, L. Wang, L. Bian, J. B. Xu, W. Ren, P. F. Hu, and A. M. Chang, *J. Power Sources* **277**, 139 (2015).
- ³⁸ A. S. Keefe, S. Buteau, I. G. Hill, and J. R. Dahn, *J. Electrochem. Soc.* **166**, A3272 (2019).
- ³⁹ Y.-C. Jin and J.-G. Duh, *J. Electrochem. Soc.* **164**, A735 (2017).
- ⁴⁰ A. V. D. Ven and G. Ceder, *Electrochem. Solid-State Lett.* **3**, 5 (2000).
- ⁴¹ L. A. Montoro and J. M. Rosolen, *Electrochim. Acta* **49**, 3243 (2004).
- ⁴² C. Ho, I. Raistrick, and R. A. Huggins, *J. Electrochem. Soc.* **127**, 343 (1980).
- ⁴³ H. Liu, C. Li, H. P. Zhang, L. J. Fu, Y. P. Wu, and H. Q. Wu, *J. Power Sources* **159**, 717 (2006).
- ⁴⁴ P. Chen, H. Wu, S. Huang, and Y. Zhang, *Ceram. Int.* **42**, 10498 (2016).
- ⁴⁵ Y. Shi, M. Zhang, C. Fang, and Y. S. Meng, *J. Power Sources* **394**, 114 (2018).
- ⁴⁶ K. Nakamura, H. Ohno, K. Okamura, Y. Michihiro, I. Nakabayashi, and T. Kanashiro, *Solid State Ionics* **135**, 143 (2000).
- ⁴⁷ J. Sugiyama, Y. Ikedo, K. Mukai, H. Nozaki, M. Månsson, O. Ofer, M. Harada, K. Kamazawa, Y. Miyake, J. H. Brewer, E. J. Ansaldo, K. H. Chow, I. Watanabe, and T. Ohzuku, *Phys. Rev. B* **82**, 1 (2010).
- ⁴⁸ M. Okubo, Y. Tanaka, H. Zhou, T. Kudo, and I. Honma, *J. Phys. Chem. B* **113**, 2840 (2009).
- ⁴⁹ H. Moriwake, A. Kuwabara, C. A. Fisher, R. Huang, T. Hitosugi, Y. H. Ikuhara, H. Oki, and Y. Ikuhara, *Adv. Mater.* **25**, 618 (2013).
- ⁵⁰ K. Kang and G. Ceder, *Phys. Rev. B* **74**, 1 (2006).
- ⁵¹ T. S. Horányi, *Thermochim. Acta* **142**, 143 (1989).
- ⁵² A. Van der Ven, D. Morgan, Y. S. Meng, and G. Ceder, *J. Electrochem. Soc.* **153**, A210 (2006).
- ⁵³ Y. F. Li and A. Selloni, *J. Phys. Chem. Lett.* **5**, 3981 (2014).
- ⁵⁴ A. J. Tkalych, K. Yu, and E. A. Carter, *J. Phys. Chem. C* **119**, 24315 (2015).